1-22-1999

Crystal structure of the H256A mutant of rat testis fructose-6-phosphate,2-kinase/fructose-2,6-bisphosphatase: Fructose 6-phosphate in the active site leads to mechanisms for both mutant and wild type bisphosphatase activities

Mi H. Yuen
UT Southwestern Medical School

Hiroyuki Mizuguchi
UT Southwestern Medical School

Yong Hwan Lee
UT Southwestern Medical School

Paul F. Cook
University of Oklahoma

Kosaku Uyeda
UT Southwestern Medical School

See next page for additional authors

Recommended Citation

Yuen, M., Mizuguchi, H., Lee, Y., Cook, P., Uyeda, K., & Hasemann, C. (1999). Crystal structure of the H256A mutant of rat testis fructose-6- phosphate,2-kinase/fructose-2,6-bisphosphatase: Fructose 6-phosphate in the active site leads to mechanisms for both mutant and wild type bisphosphatase activities. *Journal of Biological Chemistry, 274* (4), 2176-2184. https://doi.org/10.1074/jbc.274.4.2176

THE JOURNAL OF BIOLOGICAL CHEMISTRY Vol. 274, No. 4, Issue of January 22, pp. 2176–2184, 1999
Printed in U.S.A.

Crystal Structure of the H256A Mutant of Rat Testis Fructose-6-phosphate,2-kinase/Fructose-2,6-bisphosphatase

FRUCTOSE 6-PHOSPHATE IN THE ACTIVE SITE LEADS TO MECHANISMS FOR BOTH MUTANT AND WILD TYPE BISPHOSPHATASE ACTIVITIES*

(Received for publication, July 14, 1998, and in revised form, August 26, 1998)

Mi H. Yuen‡, Hiroyuki Mizuguchi§¶, Yong-Hwan Lee‡, Paul F. Cook‖, Kosaku Uyeda§¶, and Charles A. Hasemann‡§**

From the Departments of ‡Internal Medicine and §Biochemistry, University of Texas Southwestern Medical Center, Dallas, Texas 75235, ¶Research Service, Department of Veterans Affairs Medical Center, Dallas, Texas 75216, and the ‖Department of Chemistry and Biochemistry, University of Oklahoma, Norman, Oklahoma 73019

Fructose-6-phosphate,2-kinase/fructose-2,6-bisphosphatase (Fru-6-P,2-kinase/Fru-2,6-Pase) is a bifunctional enzyme, catalyzing the interconversion of β-D-fructose-6-phosphate (Fru-6-P) and fructose-2,6-bisphosphate (Fru-2,6-P_2) at distinct active sites. A mutant rat testis isozyme with an alanine replacement for the catalytic histidine (H256A) in the Fru-2,6-Pase domain retains 17% of the wild type activity (Mizuguchi, H., Cook, P. F., Tai, C-H., Hasemann, C. A., and Uyeda, K. (1998) *J. Biol. Chem.* 274, 2166–2175). We have solved the crystal structure of H256A to a resolution of 2.4 Å by molecular replacement. Clear electron density for Fru-6-P is found at the Fru-2,6-Pase active site, revealing the important interactions in substrate/product binding. A superposition of the H256A structure with the RT2K-Wo structure reveals no significant reorganization of the active site resulting from the binding of Fru-6-P or the H256A mutation. Using this superposition, we have built a view of the Fru-2,6-P_2-bound enzyme and identify the residues responsible for catalysis. This analysis yields distinct catalytic mechanisms for the wild type and mutant proteins. The wild type mechanism would lead to an inefficient transfer of a proton to the leaving group Fru-6-P, which is consistent with a view of this event being rate-limiting, explaining the extremely slow turnover (0.032 s^{-1}) of the Fru-2,6-Pase in all Fru-6-P,2-kinase/Fru-2,6-Pase isozymes.

The bifunctional enzyme fructose-6-phosphate,2-kinase/fructose-2,6-bisphosphatase (Fru-6-P,2-kinase[1]/Fru-2,6-Pase) participates in glucose homeostasis by regulating the intracellular concentration of fructose-2,6-bisphosphate (Fru-2,6-P_2). Fru-2,6-P_2 is both a potent physiological activator of 6-phosphofructokinase, and an *in vitro* inhibitor of fructose-1,6-bisphosphatase (reviewed in Refs. 2–4). There is significant sequence homology among the Fru-2,6-Pase domain, the phosphoglycerate mutases, and the acid phosphatases (5, 6). We previously determined the crystal structure of the rat testis Fru-6-P,2-kinase/Fru-2,6-Pase (RT2K-Wo), showing the enzyme to be a head-to-head homodimer of 55-kDa subunits, with each monomer consisting of independent kinase and phosphatase domains (7). The kinase domains are in close contact, forming an extended hydrophobic core between them, while the phosphatase domains are essentially independent of one another. The structure of the isolated rat liver Fru-6-P,2-kinase/Fru-2,6-Pase (RL2K) Fru-2,6-Pase domain has also been determined (8), and as would be predicted by the 85% identity between the Fru-2,6-Pase domains, the structures are nearly identical. Comparison of the RT2K-Wo Fru-2,6-Pase domain structure with those of yeast phosphoglycerate mutase (9) and rat acid phosphatase (10) confirmed that these enzymes also have very similar tertiary structures (7). These enzymes share a common catalytic mechanism involving a covalent phosphohistidine intermediate (11–14) located in a conserved sequence motif (*Z*XRHG(E/Q)*XXX*N, where *Z* is a hydrophobic residue (15)). The sequence motif ^{253}LCR**H**GESELN^{262} is found in the RT2K phosphatase domain, where His^{256} is the catalytic histidine. This conserved sequence motif, together with Arg^{305}, Glu^{325}, and His^{390}, forms a larger conserved structural motif defining the catalytic center of all three enzymes (7).

Mutagenesis and kinetic analyses on the rat liver isozyme (16–20) led to a model of Fru-2,6-P_2 binding and a potential phosphatase reaction mechanism. Thus, the catalytic histidine (His^{258} in RL2K, His^{256} in RT2K) was proposed to make a nucleophilic attack on the 2-phosphate of Fru2,6-P_2, while positively charged side chains (Arg^{257} and Arg^{307} in RL2K, Arg^{255} and Arg^{305} in RT2K) orient the 2-phosphate and stabilize the transition state. His^{392} (His^{390} in RT2K) was proposed to be coupled to Glu^{327} (Glu^{325} in RT2K), making His^{392} doubly protonated, and capable of donating a proton to the leaving group oxygen of Fru-6-P. A water, activated by Glu^{327}, would then attack the phosphoenzyme intermediate, regenerating the enzyme and producing a free PO_4 ion (8, 14). This interpretation of the mutagenesis and the proposed reaction mechanism are largely in agreement with the RT2K-Wo and RL2K Fru-2,6-Pase domain structures, with the exception of the role of

* This work was supported by grants from the Welch Foundation, the American Heart Association, Texas Affiliate (to C. A. H.), and the Department of Veterans Affairs and National Institutes of Health Grants DK16194 (to K. U.) and GM36799 (to P. F. C.). The costs of publication of this article were defrayed in part by the payment of page charges. This article must therefore be hereby marked "*advertisement*" in accordance with 18 U.S.C. Section 1734 solely to indicate this fact.

The atomic coordinates and structure factors (code 2bif) have been deposited in the Protein Data Bank, Brookhaven National Laboratory, Upton, NY.

** To whom correspondence should be addressed: Dept. of Internal Medicine, UT Southwestern Medical Center, 5323 Harry Hines Blvd., Dallas, TX 75235-8884.

[1] The abbreviations used are: Fru-6-P,2-kinase, fructose-6-phosphate,2-kinase; Fru-2,6-Pase, fructose-2,6-bisphosphatase; Fru-2,6-P_2, fructose-2,6-bisphosphate; Fru-6-P, β-D-fructose-6-phosphate; AMP-PNP, 5′-adenylyl imidodiphosphate; RL2K, rat liver isozyme of fructose-6-phosphate,2-kinase/fructose-2,6-bisphosphatase; RT2K, rat testis isozyme of fructose-6-phosphate,2-kinase/fructose-2,6-bisphosphatase; RT2K-Wo, RT2K with all four tryptophans mutated to phenylalanine; H256A, a mutant form of RT2K-Wo with an additional histidine 256 to alanine mutation.

His^{390}, which is neither coupled to Glu^{325}, nor in a position to donate a proton to Fru-6-P. It is important to note, however, that neither the RT2K-Wo nor the original RL2K Fru-2,6-Pase domain structures contained bound ligands (Fru-6-P or Fru-2,6-P_2), which has hampered a thorough characterization of the Fru-2,6-Pase mechanism. The report of a trapped RL2K phosphoenzyme intermediate (21) and the work presented here combine to remedy this deficiency.

To facilitate our own crystallographic studies of the RT2K kinase reaction, we generated a mutant protein, H256A, that as reported for the RL2K H258A mutant (16), would be devoid of phosphatase activity (and allow us to soak Fru-2,6-P_2 into crystals without consumption by the Fru-2,6-Pase reaction). This enzyme unexpectedly retains 17% of the RT2K-Wo Fru-2,6-Pase activity and led to a series of experiments to assess the basis for this activity. The results of mutagenesis and kinetic analyses on the Fru-2,6-Pase domain of the RT2K isozyme are presented in a companion paper (1). We report here the crystallographic structure of the Fru-2,6-Pase domain of the RT2K H256A mutant enzyme. This structure includes bound Fru-6-P and PO_4 ligands in the active site. Based on a comparison of the RT2K-Wo, H256A mutant, and the RL2K phosphoenzyme structures, we propose catalytic mechanisms that explain the observed kinetic data for both mutant and wild type enzymes.

EXPERIMENTAL PROCEDURES

Protein Preparation and Crystallization—The preparation and purification of the Wo form of RT2K was described previously (22, 23). A single point mutation of the Wo enzyme, converting His^{256} to Ala was generated and purified by the same procedure (1). Crystallization was performed by the hanging drop vapor diffusion method. The conditions for crystallization were a modified version of those reported previously (24). Briefly, 10 mg/ml of protein (in 50 mM Tris·PO_4, pH 7.5, 5% glycerol, 40 μM EDTA, 40 μM EGTA, 800 μM dithiothreitol, 0.4% PEG300, 1.7 mM Fru-6-P, 1.7 mM AMP-PNP, 1% β-octyl glucoside) was mixed 1:1 with a well solution of 17% polyethylene glycol 4000, 60–90 mM succinate, pH 6.0, 10% glycerol, and 10 mM $MgCl_2$. Crystals were grown and stored at 4 °C.

Data Collection and Processing—Crystals were serially transferred into solutions of surrogate mother liquor (19% PEG 4000, 10 mM $MgCl_2$, 90 mM succinate, pH 6.0, 50 mM Tris·HCl, pH 7.5, 1% β-octyl glucoside, 10 mM Fru-6-P, and 1 mM AMP-PNP) with increasing concentrations of glycerol (10–20% in 5% steps). These cryoprotected crystals were flash frozen in liquid propane and subsequently maintained at 120 K in a dry nitrogen stream using an X-Stream crystal cooler (Molecular Structure Corp). Data were collected on a DIP-2020 image plate detector (MacScience) mounted on a Rigaku rotating anode generator operated at 50 mA, 100 kV, with double mirror focusing (MacScience). Diffraction intensities were integrated using the program Denzo (25). All data were merged and scaled in Scalepack (25) and formatted for subsequent use in XPLOR (26). Automatic indexing in Denzo indicated that the crystals belong to space group P1, and postrefinement in Scalepack led to unit cell dimensions a = 61.74 Å, b = 73.51 Å, c = 76.70 Å; α = 116.9°, β = 99.31°, and γ = 105.2°. Assuming two molecules per asymmetric unit, the calculated Matthews coefficient (27) is 2.54 $Å^3$/Da.

Phasing by Molecular Replacement, Model Building, and Refinement—The rotation search and PC refinement were carried out in XPLOR, using a polyalanine model derived from the RT2K-Wo crystal structure (7). Because of the extensive interaction between monomers in the original $P3_121$ crystal form, we anticipated that the global dimer structure would be unchanged in this new P1 crystal packing and thus used the entire dimer as a search model, rather than separate searches for the two monomers. The molecular replacement was unambiguous, with a rotation function peak 7.4 σ above the mean. Rigid body minimization of this rotation solution using data from 20- to 2.8-Å resolution led to an R_{free} of 0.51 for the polyalanine model and an R_{free} of 0.42 with all side chains included. To minimize model bias, initial electron density maps were calculated with the polyalanine molecular replacement phases and data from 30 to 2.4 Å, using SIGMAA (28) weighting as implemented in XPLOR. Model rebuilding was accomplished using the program O (version 6.1 (29)). The major changes in the structure are related to changes in the ligand-binding state of both catalytic domains and changes due to crystal packing. Refinement in XPLOR included the use of noncrystallographic restraints. Four groups were defined (kinase-tight, kinase-loose, phosphatase-tight, and phosphatase-loose), using a weight of 100 for the tighter and 50 for the looser restraints. Rebuilding, positional, and B-factor refinement yielded the final model reported here with indicators of model quality as reported in Table I. Coordinates have been deposited with the Protein Data Bank (30), with accession code 2bif.

TABLE I
Structure determination statistics

Parameters	Values
Diffraction data	
Resolution (Å)	30–2.4
No. of reflections ($F \geq 2\sigma(F)$)	37,144
Completeness (%)	95.1 (93.1)
Multiplicity	2.16 (2.14)
$I/\sigma(I)$	15.6 (4.75)
R_{sym}	5.2
R_{work}	20.0
R_{free}	24.4
Model composition	
No. of amino acids	864[a]
No. of protein atoms	7017
No. of heteroatoms	153
No. of water molecules	274
No. of refinement parameters	29,776
Observations/parameter	1.25
Coordinate error (Å)	
Luzzati	0.35
SIGMAA	0.35
Stereochemistry	
Bond lengths (Å)	0.012
Bond angles (degrees)	1.60
Improper angles (degrees)	1.48
Thermal parameters	
Mean B (main chain)	33.4
Mean B (side chain)	35.7
Mean B (protein/heteroatoms)	34.8
Mean B (solvent)	27.6
Root mean square deviation B bonded	2.97
Root mean square deviation B angles	4.54
Overall B (Wilson plot)	37.4

[a] Each monomer is missing the first 36 amino acids. Thus, 864 = 2 × (468 − 36).

RESULTS

Protein Crystallization and Structure Solution—Crystals of the RT2K H256A mutant protein were grown by the hanging drop vapor diffusion method as described under "Experimental Procedures." Crystals grew with a rod-shaped morphology and were found to belong to space group P1. The unit cell dimensions are a = 61.7 Å, b = 73.5 Å, c = 76.7 Å; α = 116.9°, β = 99.31°, and γ = 105.2°, and there are two monomers (the functional dimer) in the asymmetric unit. These crystals diffract to 2.4 Å, and data were collected from specimens frozen at cryogenic (120 K) temperatures. The structure was solved by molecular replacement using the reported RT2K-Wo structure as a search model. A summary of the overall data and model qualities is presented in Table I. The overall structure of the RT2K dimer is similar to that reported earlier (7), *i.e.* a close interaction between kinase domains, with essentially independent phosphatase domains tethered to the kinase dimer. Because there are two monomers in the asymmetric unit, we have determined two independent structures of the monomer. For the kinase domains, the two copies are different, with subtle conformational changes, and different ligands bound.[2] The two phosphatase domains are quite similar in conformation and bound ligands, although one copy has generally lower B-factors (monomer A average B-factor = 50.1; monomer B average B-factor = 32.3), due to closer crystal packing for the phosphatase domain of monomer B. For this reason, subse-

[2] M. H. Yuen and C. A. Hasemann, manuscript in preparation.

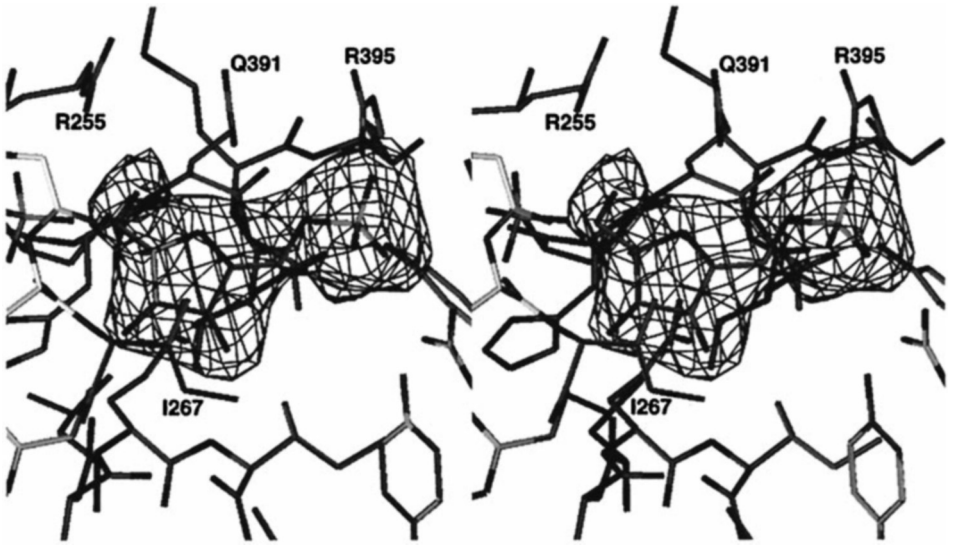

FIG. 1. **Electron density of Fru-6-P bound in the Fru-2,6-Pase active site.** A stereo view of the final molecular model of Fru-6-P bound in the Fru-2,6-Pase active site is shown, with several neighboring amino acids labeled. The electron density mesh is drawn at the 4.5σ contour of an $F_o - F_c$ difference map, calculated after Fru-6-P was omitted, and the model was subjected to 2,500 K simulated annealing in XPLOR (26). This *figure* was generated using the program O (29).

quent results and discussion will generally be restricted to the phosphatase domain of monomer B.

Fru-6-P Binding in the Active Site—In our previous structure of RT2K-Wo, there was not a Fru-6-P molecule bound to the Fru-2,6-Pase domain, despite its presence in the crystallization mixture. Instead, there were phosphate ions bound in the presumed binding sites for the 2- and 6-phosphates of Fru-6-P. In the structure of the RT2K H256A mutant reported here, there is clear electron density for Fru-6-P in both monomers (Fig. 1). The refined coordinates of the Fru-6-P molecule in the binding site (Fig. 2) reveal that the Fru-6-P traverses a crevice composed of Ile^{267}, Glu^{325}, Tyr^{336}, Arg^{350}, Lys^{354}, Tyr^{365}, Gln^{391}, and Arg^{395}. The polar residues form hydrogen bonds with the Fru-6-P hydroxyls and 6-phosphate (Table II and Fig. 2), while Ile^{267} forms a Van der Waals interaction by stacking with the fructose ring (Fig. 3). Tyr^{336}, Arg^{350}, Lys^{354}, and Tyr^{365} interact with the 6-phosphate in exactly the same way that the free phosphate was bound in the RT2K-Wo structure. Eight of the nine oxygens of Fru-6-P are involved in direct hydrogen bonds to the protein or to well ordered waters, which are in turn bound by protein. Fru-6-P-O-1 interacts with two water molecules, which are in turn bound to main chain carbonyls and side chains. Fru-6-P-O-2, which is of course the site of bond cleavage from the 2-phosphate during the Fru-2,6-Pase reaction, forms a hydrogen bond with Glu^{325}, making Glu^{325} a prime candidate for a catalytic residue, as will be discussed below. The main chain nitrogen of Gly^{268} interacts with the Fru-6-P-O-3 hydroxyl, while the nitrogen of Gln^{391} forms two hydrogen bonds to fructose oxygens (O-5 and O-6). Only Fru-6-P-O-4 is not involved in a hydrogen bond interaction, and that is because the stacking of Ile^{267} with the fructose ring includes an interaction with the C-4–O-4 bond, preventing a close approach of any other protein groups that might interact with Fru-6-P-O-4. This mode of Fru-6-P binding (a combination of many hydrogen bonds and hydrophobic stacking) is typical for carbohydrate binding proteins that bind their substrate in an internal pocket (type I proteins, as defined by Quiocho (31) and Vyas (32)) and promotes both tight binding and substrate specificity.

Phosphate Binding at the 2-Phosphate Pocket—A phosphate ion is bound in the 2-phosphate pocket of both monomers in the crystal. The phosphate is in hydrogen bonding distance to the side chains of Arg^{255}, Glu^{325}, Arg^{305}, His^{390}, Asn^{262}, and the main chain nitrogen of Gln^{391}, as well as being in contact with Fru-6-P-O-2. A superposition of the H256A and RT2K-Wo structures shows that the phosphate occupies a different position in the two enzymes. In the H256A structure, the ion shifts (by an average distance of 1.46 Å for the two monomers) to occupy the space created by the loss of His^{256}. While the phosphate still contacts the same set of protein atoms, most of the hydrogen bonds are longer in the H256A mutant (Table III). The phosphate in the H256A structure has, of course, lost its interaction with His^{256} but has gained an interaction with Fru-6-P.

Modeling Fru-2,6-P_2 Binding in the Active Site—Superposition of the H256A crystal structure with the RT2K-Wo structure allows us to generate a model of Fru-2,6-P_2 in the phosphatase active site. This is possible because the positions of the 6-phosphate and protein atoms in the active site have not changed (root mean square coordinate change for 143 atoms = 0.20 Å) beyond the intrinsic coordinate error of the H256A model (0.35 Å). Thus, by combining the protein and 2-phosphate analogue from the RT2K-Wo structure with the Fru-6-P from the H256A structure, we achieve an excellent approximation of the Fru-2,6-P_2 complex (Fig. 3). The arrangement of protein/Fru-6-P hydrogen bonds and Van der Waals interactions described above holds the Fru-2,6-P_2 molecule in the ideal orientation for an in-line associative transfer of the 2-phosphate to His^{256}. Thus, the crystallographically determined location of Fru-6-P in the active site (and the model of Fru-2,6-P_2) allow us to re-evaluate the proposed catalytic mechanism in more detail.

DISCUSSION

Fru-6-P and Fru-2,6-P_2 Binding—The structure presented here represents the first structure of a Fru-6-P-bound form of an intact Fru-2,6-Pase domain in a dimeric Fru-6-P,2-kinase/Fru-2,6-Pase. Fru-6-P is a potent inhibitor of Fru-2,6-Pase activity at physiologic concentrations of Fru-6-P (K_i = 51 nM, hepatocyte concentration of 20–50 μM). In the case of the RT2K isozyme, this should result in an inhibited Fru-2,6-Pase activity and a net production of Fru-2,6-P_2 and consequent driving force for glycolysis in tissues that express this isozyme. Thus, the elucidation of the mode of binding of this potent inhibitor is itself significant. Recently, a structure of the truncated form of

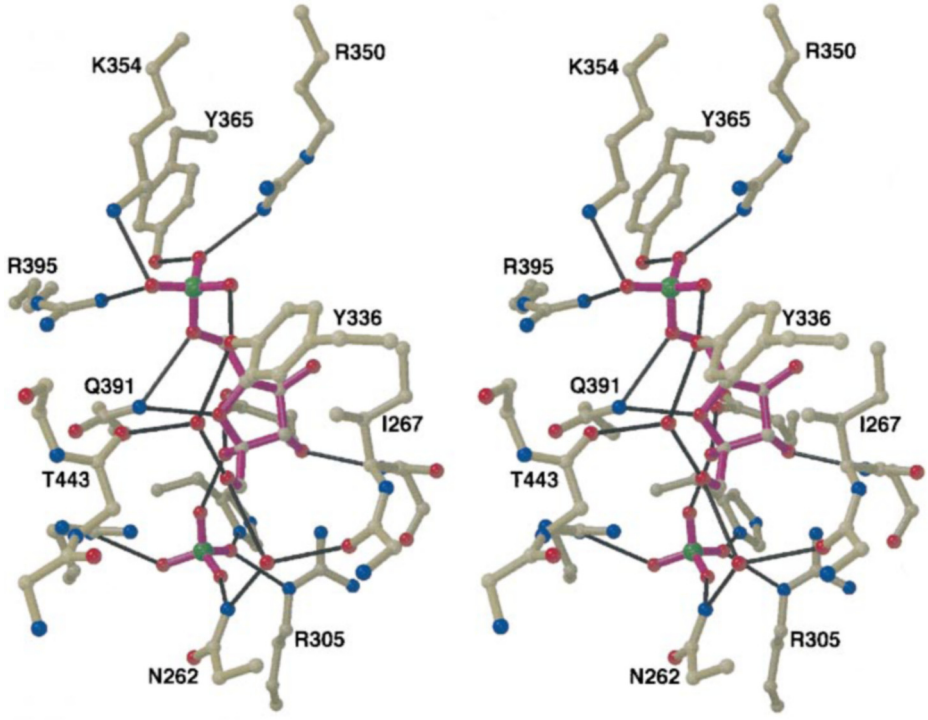

FIG. 2. **Fru-6-P interactions in the Fru-2,6-Pase active site.** A stereo view of the Fru-2,6-Pase active site is shown, with the protein bonds *colored tan*, and the Fru-6-P and phosphate bonds *magenta*. The various interactions between protein and Fru-6-P that account for the affinity and specificity of the active site are shown. The Fru-6-P 6-phosphate is shown at the *top*, bound by interactions with Arg^{350}, Lys^{354}, Tyr^{365}, and Arg^{395}. The fructose portion of Fru-6-P is bound by both hydrogen bonds and a hydrophobic stacking interaction, where Ile^{267} can be seen to stack with the fructose ring and Fru-6-P-O-2. The amide nitrogen of Gln^{391} has a bidentate interaction with the fructose at O-5 and O-6. The main chain nitrogen of Ile^{267} is hydrogen-bonded to Fru-6-P-O-3. The two water molecules that form hydrogen bonds between Fru-6-P-O-1 and the protein are shown as isolated *red spheres*. One of these waters interacts with Fru-6-P, Tyr^{336}, and the main chain carbonyl of Thr^{443}. The other water interacts with Asn^{262} and the main chain carbonyl of position 266. The free phosphate (analogous to the 2-phosphate of Fru-2,6-P_2) is shown at the *bottom*, bound by Arg^{255}, Asn^{262}, Arg^{305}, and His^{390}. The identities of the side chains are indicated with the one-letter amino acid designation and position in the RT2K protein sequence. The side chain of Thr^{443} has not been included so as not to obscure the view of F-6-P. Not labeled and at the back of the image are Arg^{255}, Glu^{325}, and His^{390}, interacting with the Fru-6-P molecule and/or the free phosphate. Hydrogen bonds between the Fru-6-P, phosphate, and protein are drawn as *black lines*. This figure was produced using MOLSCRIPT (40) and rendered in Raster3D (41).

TABLE II
Fru-6-P interaction with the RT2K H256A mutant

Fru-6-P	Fru-6-P,2-kinase/Fru-2,6-Pase		
	Residue and atom	Contact distance	
		Monomer A	Monomer B
		Å	
O-2	Glu^{325} Oϵ2	2.83	2.60
O-3	Gly^{268} N	3.03	2.86
O-5	Gln^{391} Nϵ2	2.62	2.73
O-6	Gln^{391} Nϵ2	3.19	3.06
O-61	Tyr^{365} Oη	2.78	2.70
	Arg^{350} Nη2	2.65	2.69
O-62	Arg^{395} Nη1	2.76	2.92
	Lys^{354} Nζ	2.86	2.59
O-63	Tyr^{336} Oη	2.75	2.78
	Arg^{350} Nη1	3.17	3.36
C-3, C-4, O-4, C-5	Ile^{267} Cα, Cβ, Cγ2	3.8–4.1	3.6–4.2

an isolated RL2K Fru-2,6-Pase domain was determined with a covalent phosphohistidine intermediate in the presence of Fru-6-P (21). The position of the Fru-6-P molecule is notably different in the two structures. While it is impossible to say that one conformation is correct and the other incorrect, there are several points that argue that the conformation of Fru-6-P reported here is more likely to be the native conformation. First, the RL2K structures are of a truncated protein that is missing 30 C-terminal amino acids. The analogous stretch of polypeptide in our RT2K structure passes within 3.5 Å of the Fru-6-P molecule, at Thr^{443}. The carbonyl oxygen of Thr^{443} is in fact hydrogen-bonded to a water, which in turn coordinates the 1-hydroxyl of Fru-6-P (see Fig. 2). In addition, the region of RL2K structure that should have been occupied by the truncated protein is instead involved in a crystal contact, such that amino acids from a neighboring molecule are within 5.8 Å of the Fru-6-P. One of these amino acids (Gln^{342}) actually interacts with Gln^{393} (the analogue of Gln^{391} in RT2K). Remember that Gln^{391} makes two hydrogen bonds with Fru-6-P that are important in maintaining its position in the active site (see Fig. 2). Last, the Fru-6-P in the RL2K structure is in an unusual conformation compared with two Fru-6-P and two Fru-1,6-P_2 structures from the Cambridge small molecule data base. In contrast, the Fru-6-P conformation reported here closely resembles the extended, low energy conformations determined by small molecule crystallography. Finally, recall that Ile^{267} forms a typical stacking interaction with the fructose ring in the structure reported here. This stacking interaction is absent in the RL2K structure.

The determination of a Fru-6-P-bound form of the RT2K H256A Fru-2,6-Pase domain has allowed us to build a reliable model of the Fru-2,6-P_2-bound enzyme. As seen in Fig. 3, the active site of the Fru-2,6-Pase domain is perfectly tailored to accommodate Fru-2,6-P_2. The active site serves as a molecular ruler, measuring the length of the bound substrate along an axis defined by the line between the Fru-6-P 2-hydroxyl and His^{256} (5.5 Å in the RT2K-Wo structure; see Fig. 4). In this space, there is room for one phosphate, one covalent bond to phosphate (1.6–1.8 Å), and one noncovalent interaction (~3.2 Å). Thus, Fru-2,6-P_2 is accommodated, with a covalent Fru-6-P-2-phosphate bond and the 2-phosphate in Van der Waals contact with His^{256}. After the catalytic transfer of the 2-phosphate to His^{256}, the ruler is still satisfied, with a covalent

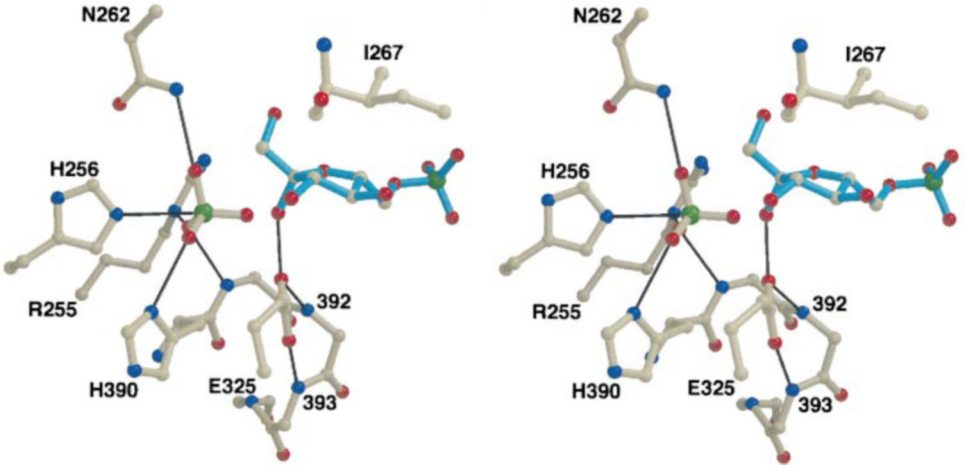

FIG. 3. **Model of Fru-2,6-P_2 bound to the RT2K-Wo active site.** We have constructed a model of Fru-2,6-P_2 binding to the Fru-2,6-Pase active site based on the coordinates of the RT2K-Wo structure (protein and 2-phosphate drawn with *tan bonds*) and the coordinates of Fru-6-P from the H256A structure (Fru-6-P drawn with *cyan bonds*). We have not repositioned either the 2-phosphate or the Fru-6-P, so there is a small (0.9-Å) gap between the Fru-6-P-O-2 and the phosphate oxygen. This gap would obviously not exist in Fru-2,6-P_2, since these represent the same oxygen. The catalytic His^{256} is positioned in-line with the O-2–P bond, while Asn^{262}, His^{390}, and Arg^{255} are arranged perpindicular to that line, in a position to interact with the equatorial oxygens in the pentacoordinate transition state. Arg^{305} is not shown, to reduce the clutter in the figure but would be positioned in the foreground, interacting with the phosphate oxygen that is shown interacting with His^{390}. Glu^{325} is shown hydrogen-bonded with Fru-6-P-O-2 and also interacting with the N terminus of helix α14 (labeled as *392* and *393*). Ile^{267} is included to clearly demonstrate the stacking interaction between this side chain and the Fru-6-P. The identity of the side chains are indicated with the one-letter amino acid designation and position in the RT2K protein sequence. This *figure* was produced using MOLSCRIPT (40) and rendered in Raster3D (41).

TABLE III
Comparison of PO_4 interaction in RT2K-Wo and RT2K-H256A mutant (monomer B)

PO_4	Residue and atom	Distance	
		RT2K-Wo	RT2K-H256A
		Å	
O-1	Arg^{255} Nη2	3.13	3.26
	Arg^{255} Nϵ	2.97	2.91
	Gln^{391} N	2.92	4.04
	His^{256} Nϵ2	2.64	
P	His^{256} Nϵ2	3.17	
O-2	Glu^{325} Oϵ2	2.55	3.91
	Fru-6-P O-2		2.46
O-3	Arg^{305} Nη2	2.74	3.34
	Arg^{305} Nϵ	2.75	2.61
	His^{390} Nδ1	2.90	2.85
O-4	Asn^{262} Nδ2	2.97	3.14

phosphohistidine and a noncovalent interaction between the transferred 2-phosphate and Fru-6-P. However, there is not enough room for either the combination of phosphohistidine, hydrolytic water, and Fru-6-P or for a noncovalently bound phosphate ion with a Fru-6-P molecule. In those cases, the ruler would be measuring two noncovalent interactions, a distance that cannot be accommodated. The arrangement of molecules in the RL2K trapped phosphohistidine structure described above (*E*-P·H_2O·Fru-6-P) is an arrangement that violates this molecular ruler concept. This violation is only allowed because of the unnatural position of Fru-6-P in the binding pocket, which is a consequence of the C-terminal truncation of the RL2K Fru-2,6-Pase domain.

Correlation of Structures with Kinetics—The molecular ruler concept predicts an ordered reaction mechanism (Scheme I), where Fru-6-P release must precede phosphohistidine hydrolysis. After Fru-6-P has dissociated, a water molecule would be accommodated in the active site for hydrolysis of the *E*-P intermediate. This model is consistent with previous kinetic experiments where it has been reported that the rate of phosphoenzyme formation is greater than the overall reaction rate (33), that Fru-6-P inhibits the Fru-2,6-Pase reaction (34), that Fru-6-P release is the rate-limiting step in the overall reaction (35), and that P_i accelerates *E*-P hydrolysis by competing for Fru-6-P binding (presumably at the 6-phosphate binding site) (33). In our own studies, we showed that Fru-6-P release and phosphohistidine breakdown occur in parallel in the wild type enzyme (1). Together, the structural and kinetic data indicate that *E*-P hydrolysis does not occur until after Fru-6-P has dissociated from the enzyme, and that *E*-P hydrolysis is fast (Scheme 1).

There have been several models of Fru-2,6-Pase catalysis proposed, based first on mutagenesis directed by the homology of the Fru-2,6-Pase domain to the phosphoglycerate mutase family (16, 17) and later based on crystal structures (1, 7, 8, 21). These studies have all concluded that all of the amino acids that define the 2-phosphate binding pocket (His^{256}, His^{390}, Arg^{255}, Arg^{305}, Asn^{262}, and Glu^{325}) are influential in catalysis. Specifically, His^{256} has conclusively been demonstrated to act as a nucleophile that attacks the 2-phosphate, resulting in a His^{256} phosphohistidine intermediate (1, 13, 14, 21). His^{256} is perfectly placed for an in-line attack that would break the O-2–P-2 bond of Fru-2,6-P_2 with an inversion of phosphate geometry (Fig. 3). Our own data on the retention of significant catalytic activity in the H256A mutant (1) are contradictory to previous findings in the RL2K enzyme (16) and indicate that this phosphoenzyme intermediate is not an obligatory intermediate for the enzyme. Arg^{255} and Arg^{305} have been proposed to neutralize the charge of the 2-phosphate and/or to stabilize the transition state (1, 18), consistent with their location as equatorial ligands to the 2-phosphate. Glu^{325} has been proposed to act both to promote the protonation of His^{390} and to polarize a water molecule as a nucleophile for attack on the phosphohistidine intermediate (8, 17, 21). The capacity of Glu^{325} to alter

$$E + \text{Fru-2,6-P}_2 \longleftrightarrow E\bullet\text{Fru-2,6-P}_2 \xrightarrow{H^+} E\text{-P}\bullet\text{Fru-6-P} \longleftrightarrow E\text{-P} + \text{Fru-6-P} \xrightarrow{OH^-} E + \text{Pi} + \text{Fru-6-P}$$

SCHEME 1

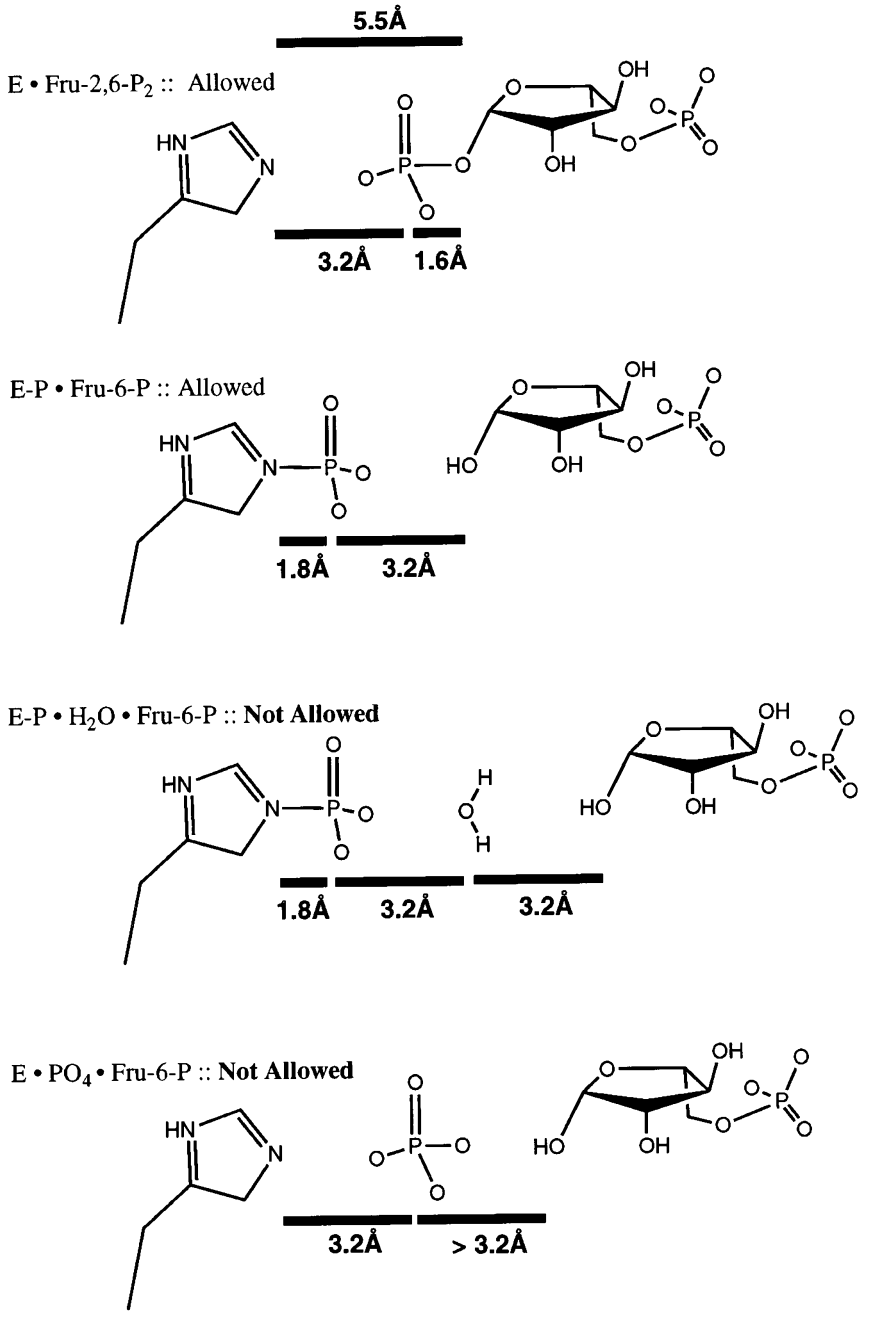

FIG. 4. **The "molecular ruler" of the Fru-2,6-Pase active site.** Based on the position of Fru-6-P in the Fru-2,6-Pase active site, there is a 5.5-Å distance between the reactive nitrogen of the catalytic histidine and the 2-OH of Fru-6-P (shown as the *dark bar* at the *top*). This distance can accommodate either an *E*·Fru-2,6-P_2 or *E*-P·Fru-6-P complex but would preclude either an *E*-P·H_2O·Fru-6-P or *E*·P·Fru-6-P complex. The *dark bars below* each complex represent ideal bond lengths or approximate Van der Waals contact distances.

the pK_a of His^{390} is doubtful, since the ionizable groups of these amino acids are not near each other (see Figs. 2 and 3). The role for Glu^{325} as a catalytic base in phosphohistidine hydrolysis is consistent with both its location in the structure and the available kinetic data on Glu^{325} mutants (1, 17). Finally, His^{390} has been proposed to act as a catalytic acid, donating a proton to the leaving group O-2 of Fru-6-P (8, 16). This, however, is inconsistent with the structure, since His^{390} is not in the vicinity of the leaving group (Fig. 3), nor does it exist in an environment that would promote its protonation. Our kinetic data from the H390A mutant protein are also inconsistent with its role as a proton donor to the leaving group, in that this mutant protein demonstrates a lag in phosphate release after Fru-6-P release (1), indicating that His^{390} is involved in phosphohistidine hydrolysis. Thus, the role of H390, the mechanism of catalysis in the H256A mutant, and the identity of the proton donor for the leaving group O-2 of Fru-6-P remain unresolved from previous findings. We believe that the Fru-2,6-Pase kinetic data (as cited above) and the structural findings reported here lead to a complete catalytic mechanism for the wild type enzyme and a distinct mechanism for the H256A mutant enzyme.

Wild Type Mechanism—Fig. 5 shows a Fru-2,6-Pase catalytic cycle where Glu^{325} is the sole amino acid involved in proton exchanges. At the beginning of the cycle (*E*·Fru-2,6-P_2 from Scheme I), His^{256} attacks the phosphate, leading to a pentacoordinate transition state, with the excess negative charge of the transition state being stabilized by Arg^{255}, Asn^{262}, Arg^{305}, and His^{390}. A protonated Glu^{325} then donates a proton to the leaving Fru-6-P. As discussed above, Fru-6-P dissociation must precede the next step, where the ionized Glu^{325} polarizes a water molecule for attack on the phosphohistidine intermediate, regenerating the ground state of the enzyme. The attractive features of this model are its simplicity and its consistency with both the kinetic and structural data. The proximity of Glu^{325} to the 2-oxygen of Fru-6-P and/or the model of Fru-

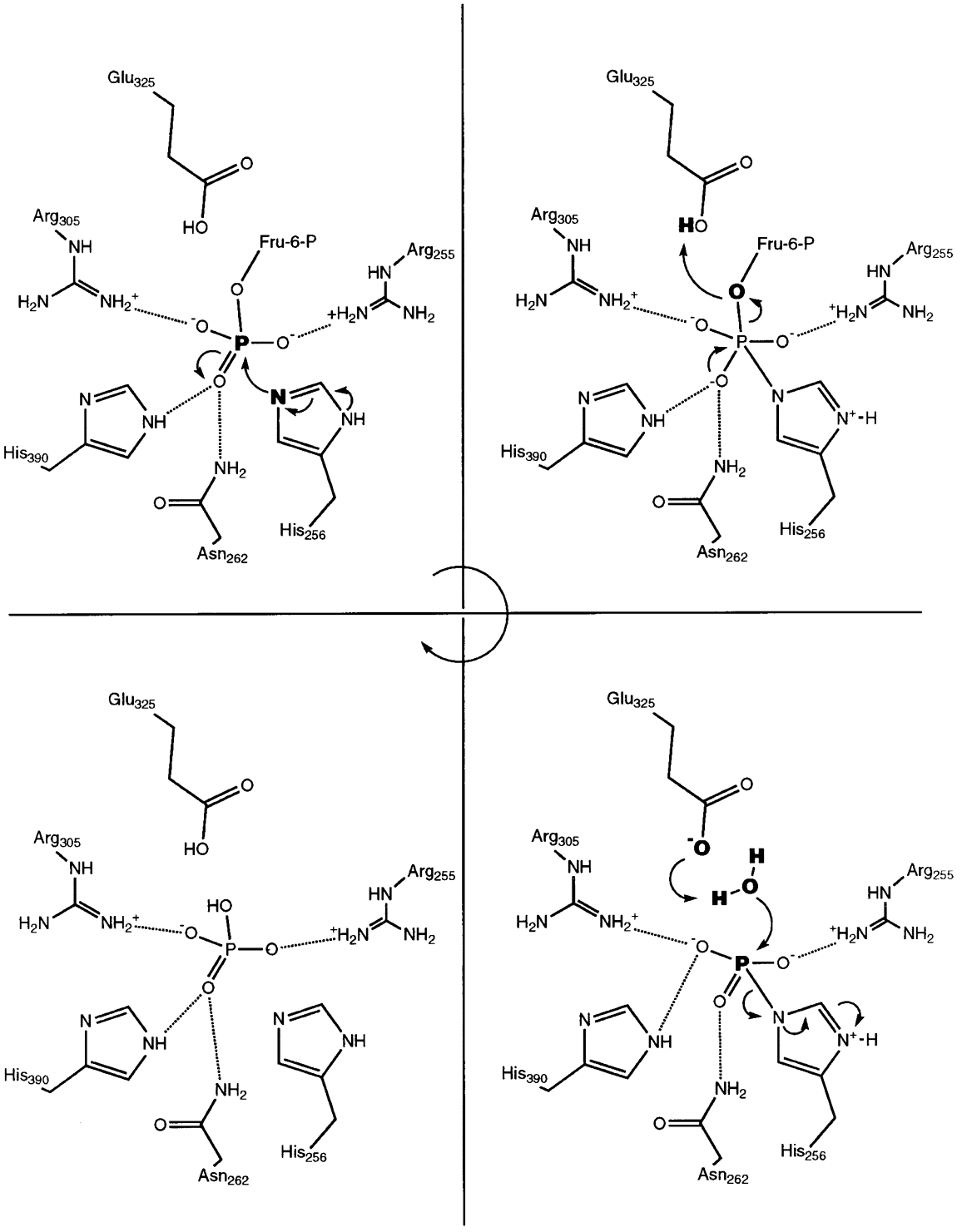

FIG. 5. **Fru-2,6-Pase catalytic cycle.** The proposed mechanism begins with formation of the *E*·Fru-2,6-P_2 complex shown in the *upper left panel*. His^{256} attacks the 2-phosphate, resulting in a tetrahedral intermediate that is stabilized by its interactions with Arg^{305}, Arg^{255}, His^{390}, and Asn^{262} as shown in the *upper right panel*. A proton derived from Glu^{325} then joins the leaving group Fru-6-P as the O-2–P bond is broken. The resulting *E*-P·Fru-6-P complex is stable, and Fru-6-P release from the active site is rate-limiting. After Fru-6-P diffuses out of the active site, a water molecule will diffuse in. Glu^{325} then activates the water as a nucleophile to attack the *E*-P intermediate as shown in the *lower right panel*. The *E*-P hydrolysis requires the formation of another tetrahedral intermediate, again stabilized by Arg^{305}, Arg^{255}, His^{390}, and Asn^{262} (not shown). Finally, the free phosphate remains bound in the 2-phosphate binding site (*lower left panel*) until it is displaced by another molecule of Fru-2,6-P_2, restarting the cycle.

2,6-P_2 and the kinetic data from Glu^{325} mutants that show a drastic loss of Fru-2,6-Pase activity (1, 17) make Glu^{325} a prime candidate for a major role in catalysis. Glu^{325} is well positioned for proton transfer to the 2-oxygen of Fru-6-P (Fig. 3, and Table II) and is well positioned to polarize water for attack on the phosphohistidine intermediate (21). The role of the amino acids that are equatorial ligands in transition state stabilization is consistent with the decreases in k_{cat}/K_m that are observed when they are mutated to amino acids that cannot fill this role. Where it has been studied, mutation of these equatorial ligands clearly affects both transition states (*i.e.* phosphohistidine formation and phosphohistidine hydrolysis). Note that His^{390},

which had previously been designated as a proton donor, is now simply another equatorial ligand. This is consistent with the kinetic data, where His^{390} mutations have effects similar to the mutation of other equatorial ligands. Most important though, is the observation that the H390A mutation causes a significant lag in P_i release after Fru-6-P release (1). This lag in P_i release is consistent with the role of His^{390} in transition state stabilization but not consistent with His^{390} as a proton donor to Fru-6-P.

There is one significant problem with this mechanism. The crystal structure clearly shows that Glu^{325} is capping the N terminus of an α-helix (α14, amino acids 391–400, Fig. 3). Such a protein environment would shift the pK_a of Glu^{325} such that the existence of a protonated Glu^{325} is unlikely, making it a poor choice for the proton donor in Fru-6-P release. On the other hand, this is in fact an enzyme with a low turnover (*i.e.* the wild type RT2K Fru-2,6-Pase reaction has a k_{cat} of 0.032 s^{-1}). Because the biological role of the enzyme is regulatory and is not a step in a biosynthetic pathway, it makes some teleological sense that the enzyme would be slow. As such, a rare protonation of Glu^{325} and subsequent proton donation to Fru-6-P could be tolerated. This idea of a slow Glu^{325} protonation is not in agreement with the kinetic evidence, however, since phosphohistidine formation has been reported to be 2 orders of magnitude faster than the overall rate of catalysis, with the Fru-6-P release rate-limiting (34, 35). It is possible that Fru-2,6-P_2 binding to the active site shifts the Glu^{325} pK_a via the interaction of the 2-phosphate with the N terminus of helix α14 (Fig. 3).

One approach to address this apparent Glu^{325} paradox would be pH titration kinetics of phosphohistidine formation in the wild-type and active site mutant enzymes to determine the pK_a values for Glu^{325} and other active site residues. Pilkis and co-workers reported the pH titration of k_{cat}/K_m for wild type, H392A, and E327Q mutant forms of the RL2K enzyme (36). Their results with the wild type eznyme indicated two ionizable groups with pK_a values of 6.1 and 8.4, which we would interpret as the pK_a of a Fru-2,6-P_2 phosphate and an unidentified residue of the protein, respectively. The titration profiles of the H392A and E327Q mutants clearly showed a partial change in the low end pK_a with an increase in the pK_a. The curves were complex however, suggesting the possibility of compensating charge interactions. It is evident that further experiments in this area will be necessary to clarify the role of ionizable groups in the Fru-2,6-P_2ase active site.

H256A Catalysis: Hydrolysis Versus Phosphohistidine 390—The discovery that the H256A mutant of RT2K has 17% of the wild type bisphosphatase activity has led to two alternative explanations of the mechanism (1). Either the enzyme is able to utilize His^{390} as an alternate to His^{256} as a nucleophile to form a phosphohistidine 390 intermediate, or another as yet undetermined mechanism exists for the H256A mutant. Examination of the active site structure (Fig. 3) leads to the conclusion that the transfer of a phosphate to His^{390} is quite unlikely. As noted above, His^{256} is ideally positioned for the in-line transfer of phosphate from Fru-2,6-P_2. His^{390}, on the other hand, is nearly 90° off this transfer axis, ideal positioning for an equatorial ligand to the transition state intermediate, but horribly suited for an in-line phosphotransfer. In order to accomplish a phosphotransfer to His^{390}, either by direct in-line attack or by an attack from the side followed by pseudorotation (37, 38), the substrate and/or His^{390} would have to be repositioned in the active site. The position of His^{390} is of course constrained by the fold of the protein and thus could not move from its equatorial location to an axial position. Manual remodeling of Fru-6-P in the active site to a position that would lead to an axial His^{390} led only to steric clashes of Fru-6-P with protein. From this evidence, combined with the inability to detect a phosphohistidine intermediate in the H256A mutant by several methods (1), we conclude that a phosphohistidine 390 intermediate pathway is not at all likely.

An alternative hypothesis is that the H256A mechanism involves the direct hydrolysis of Fru-2,6-P_2 by water. Due to the deletion of His^{256}, there is a hole in the enzyme where the imidazole ring used to be. In the crystal structure, this hole is occupied by a free phosphate as described above (Fig. 2 and Table III). When we model Fru-2,6-P_2 bound to the enzyme by superimposing the H256A and RT2K-Wo structures, this hole would be empty in the H256A substrate complex. Since vacuums do not exist in proteins, this space will be filled, and most likely by a water molecule. Like the imidazole of His^{256}, this water molecule would be in the perfect position for an in-line transfer of the phosphate. The equatorial ligands to the phosphate remain in the same position in both the RT2K-Wo and H256A structures, so they would be competent to stabilize this hydrolytic transition state in the mutant enzyme. The best experiment to verify this hypothesis would be to utilize a synthetic Fru-2,6-P_2 that has been triply labeled at the 2-phosphate with ^{16}O, ^{17}O, and ^{18}O, generating a chiral phosphate. In the event of a direct hydrolysis, there will be an inversion of the phosphate stereochemistry, while for a two-step process involving a phosphohistidine intermediate, there will be retention of stereochemistry. Such an experiment was used to verify the phosphohistidine intermediate in phosphoglycerate mutase (39).

Acknowledgments—We thank Cu Nguyen and Yang Li for excellent technical assistance in the preparation of the enzyme, and the Howard Hughes Medical Institute x-ray facility for access to diffraction equipment.

REFERENCES

1. Mizuguchi, H., Cook, P. F., Tai, C-H., Hasemann, C. A., and Uyeda, K. (1998) *J. Biol. Chem.* **274,** 2166–2175
2. Uyeda, K. (1991) in *Study of Enzymes II* (Kuby, S. A., ed) pp. 445–456, CRC Press, Inc., Boca Raton, FL
3. Pilkis, S. J., Claus, T. H., Kurland, I. J., and Lange, A. J. (1995) *Annu. Rev. Biochem.* **64,** 799–835
4. Rousseau, G. G., and Hue, L. (1993) *Prog. Nucleic Acid Res. Mol. Biol.* **45,** 99–127
5. Fothergill-Gilmore, L. A., and Watson, H. C. (1989) *Adv. Enzymol.* **62,** 227–313
6. Bodansky, O. (1972) *Adv. Clin Chem.* **15,** 43–147
7. Hasemann, C. A., Istvan, E. S., Uyeda, K., and Deisenhofer, J. (1996) *Structure* **4,** 1017–1029
8. Lee, Y-H., Ogata, C., Pflugrath, J. W., Levitt, D. G., Sarma, R., Banaszak, L. J., and Pilkis, S. J. (1996) *Biochemistry* **35,** 6010–6019
9. Winn, S. I., Watson, H. C., Harkins, R. N., and Fothergill, L. A. (1981) *Phil. Trans. R. Soc. Lond.* **293,** 121–130
10. Schneider, G., Lindqvist, Y., and Vihko, P. (1993) *EMBO J.* **12,** 2609–2615
11. Rose, Z. B. (1970) *Arch. Biochem. Biophys.* **140,** 508–513
12. Van Etten, R. L. (1977) *Arch. Biochem. Biophys.* **183,** 250–259
13. Pilkis, S. J., Walderhaug, M., Murray, K., Beth, A., Venkataramu, S. D., Pilkis, J., and El-Maghrabi, M. R. (1983) *J. Biol. Chem.* **258,** 6135–6141
14. Okar, D. A., Kakalis, L. T., Narula, S. S., Armitage, I. M., and Pilkis, S. J. (1995) *Biochem. J.* **308,** 189–195
15. Pilkis, S. J., Lively, M. O., and El-Maghrabi, M. R. (1987) *J. Biol. Chem.* **262,** 12672–12675
16. Tauler, A., Lin, K., and Pilkis, S. J. (1990) *J. Biol. Chem.* **265,** 15617–15622
17. Lin, K., Li, L., Correia, J. J., and Pilkis, S. J. (1992) *J. Biol. Chem.* **267,** 6556–6562
18. Lin, K., Li, L., Correia, J. J., and Pilkis, S. J. (1992) *J. Biol. Chem.* **267,** 19163–19171
19. Li, L., Lin, K., Correia, J. J., and Pilkis, S. J. (1992) *J. Biol. Chem.* **267,** 21588–21594
20. Li, L., Lin, K., Correia, J. J., and Pilkis, S. J. (1992) *J. Biol. Chem.* **267,** 16669–16675
21. Lee, Y-H., Olson, T. W., Ogata, C. M., Levitt, D. G., Banaszak, L. J., and Lange, A. J. (1997) *Nat. Struct. Biol.* **4,** 615–618
22. Watanabe, F., Jameson, D. M., and Uyeda, K. (1996) *Protein Sci.* **5,** 904–913
23. Tominaga, N., Minami, Y., Sakakibara, R., and Uyeda, K. (1993) *J. Biol. Chem.* **268,** 15951–15957
24. Istvan, E. S., Hasemann, C. A., Kurumbail, R. G., Uyeda, K., and Deisenhofer, J. (1995) *Protein Sci.* **4,** 2439–2441
25. Otwinowski, Z., and Minor, W. (1997) *Methods Enzymol.* **276,** 307–326
26. Brünger, A. T. (1993) *X-PLOR Version 3.1: A System for Crystallography and NMR,* Yale University Press, New Haven, CT
27. Matthews, B. W. (1968) *J. Mol. Biol.* **33,** 491–497

28. Read, R. J. (1986) *Acta Crystallogr. Sec. A* **42,** 140–149
29. Jones, T. A., Zou, J. -Y., Cowan, S. W., and Kjeldgaard, M. (1991) *Acta Crystallogr. Sec. A* **47,** 110–119
30. Bernstein, F. C., Koetzle, T. F., Williams, G. J. B., Meyer, E. F., Brice, M. D., Rodgers, J. R., Kennard, O., Shimanouchi, T., and Tasumi, M. (1977) *J. Mol. Biol.* **112,** 535–542
31. Quiocho, F. A. (1993) *Biochem. Soc. Trans.* **21,** 442–448
32. Vyas, N. K. (1991) *Curr. Opin. Struct. Biol.* **1,** 732–740
33. Stewart, H. B., El-Maghrabi, M. R., and Pilkis, S. J. (1985) *J. Biol. Chem.* **260,** 12935–12941
34. Pilkis, S. J., Regen, D. M., Stewart, H. B., Pilkis, J., Pate, T. M., and El-Maghrabi, M. R. (1984) *J. Biol. Chem.* **259,** 949–958
35. Stewart, H. B., El-Maghrabi, M. R., and Pilkis, S. J. (1986) *J. Biol. Chem.* **261,** 8793–8798
36. Lin, K., Kurland, I. J., Li, L., Lee, Y-H., Okar, D., Marecek, J. F., and Pilkis, S. J. (1994) *J. Biol. Chem.* **269,** 16953–16960
37. Berry, R. S. (1960) *J. Chem. Phys.* **32,** 933–938
38. Dennis, E. A., and Westheimer, F. H. (1966) *J. Am. Chem. Soc.* **88,** 3432–3433
39. Blättler, W. A., and Knowles, J. R. (1980) *Biochemistry* **19,** 738–743
40. Kraulis, P. J. (1991) *J. Appl. Crystallogr.* **24,** 946–950
41. Merritt, E. A., and Murphy, M. E. P. (1994) *Acta Crystallogr. Sec. D* **50,** 869–873